
Diagnosis of High-Temperature Implosions Using Low- and High-Opacity Krypton Lines

High-temperature laser target implosions can be achieved by using relatively thin-shell targets. Electron temperatures of up to 5 keV at modest compressed densities (~ 1 to 5 g/cm^3) are predicted for such experiments and have been diagnosed in an initial series of implosion experiments on the upgraded OMEGA laser (see the previous article). The corresponding ion temperatures are predicted to be higher, peaking above 10 keV at the target center. The possibility of using krypton doping for diagnosing the core temperature of imploding targets was discussed in an earlier issue of the LLE Review.¹ In that work, a simplified analysis for the case of optically thick lines was performed, using approximate Stark profiles. In the present work, the use of detailed Kr Stark profile calculations by C. F. Hooper *et al.* from the University of Florida improves and extends the earlier analysis. The use of krypton doping is a powerful technique for diagnosing target implosions, as the implosion dynamics are to lowest order independent of doping and different levels of doping can be used to permit the measurement of different quantities. For example, low doping levels allow low-opacity lines to be used to measure the ion temperature via Doppler broadening, while higher doping levels allow the density-radius product (ρR) of the compressed fuel to be measured from high-opacity lines. In high-density implosions, low-opacity lines can be used to diagnose the density through Stark broadening, and higher-opacity lines can be used to estimate the extent of mixing.¹

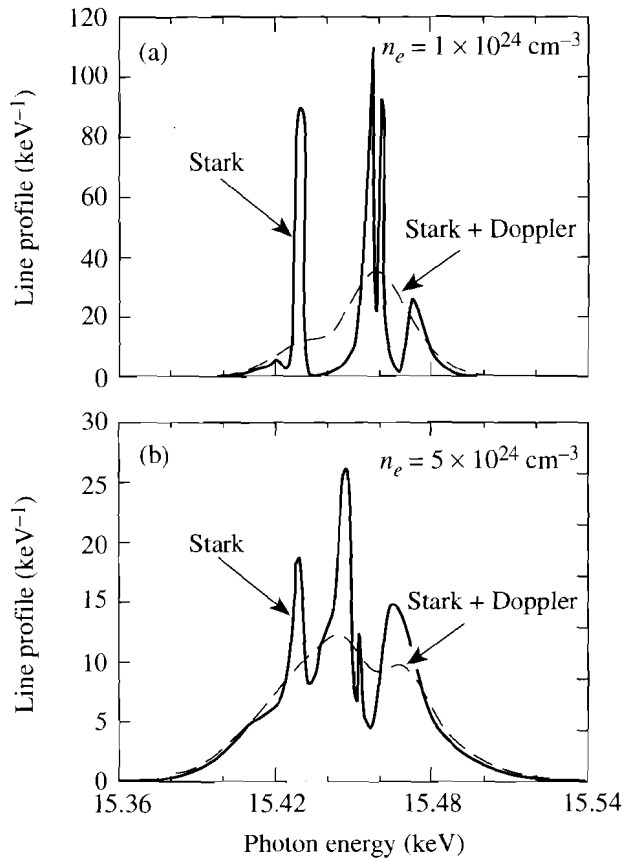
Calculations have been carried out using the *LILAC* code for a CH shell of 1-mm diameter and 10- μm thickness, filled with a 10-atm pressure of DT.¹ The laser energy was 30 kJ in a Gaussian pulse of 650-ps width. Results have shown that the core electron temperature and density are fairly uniform, at $\sim 5 \text{ keV}$ and $\sim 4.5 \text{ g/cm}^3$, respectively. On the other hand, the ion temperature ranges from $\sim 6 \text{ keV}$ to $\sim 12 \text{ keV}$ and is centrally peaked. Code calculations have shown that the core temperatures are hardly changed by the addition of 0.01 atm of krypton. By adding 0.1 atm of krypton, the peak electron temperature drops a little to about 4 keV. The predicted spectra have been calculated by the *LILAC* code and a non-LTE post-processor, which includes transitions between actual atomic

configurations, using Doppler and Stark profiles. The calculated line intensities even for the 0.01-atm case are very substantial (of the order of 10^{17} keV/keV), and the contrast of line to continuum is better than a factor of 4 for the He- β line. Furthermore, the shape of the spectrum above $\sim 10 \text{ keV}$ at peak compression differs little from the time-integrated spectrum because most of the emission originates from peak compression. Thus, a time-integrated measurement in this spectral range yields the conditions at peak compression with reasonable reliability.¹

Diagnosis of Density Using Low-Opacity Lines

A recently developed multielectron line-profile formalism and code (MERL)^{2,3} has been used to calculate Stark-broadened emission line profiles for the Kr K-shell lines. The analysis in this article relies in particular on the helium- β transition (3^1P-1^1S), and the profiles shown here pertain to this line. Broadening due to perturbing ions is treated in the quasi-static ion approximation, and the dynamic effect of electrons is calculated using a second-order relaxation theory. Ion- and electron-radiator interactions are computed in the dipole approximation. Necessary atomic physics data (energy-level structure and reduced dipole matrix elements) were calculated using Cowan's⁴ multiconfiguration atomic structure code, using the Hartree-Plus-Statistical-Exchange method for approximating the potential energy function due to the electrons, and including relativistic corrections.

Figure 64.15 shows examples of calculations carried out by the group at the University of Florida. The Stark profile of the helium- β line of Kr^{+34} , of 0.8033- \AA wavelength, is calculated for two densities: (a) $1 \times 10^{24} \text{ cm}^{-3}$ and (b) $5 \times 10^{24} \text{ cm}^{-3}$. It is assumed that the krypton constitutes a small fraction mixed into the fuel and that most of the perturbers are fuel ions. The effect of Doppler broadening is also calculated, at an assumed ion temperature of 10 keV. The shape of the Stark profile is significantly affected by relativistic effects in the atomic physics due to the relatively high nuclear charge Z of krypton. There are two dipole-allowed transitions from the $1s3l$ upper-level manifold to the ground state. The unperturbed singlet-singlet



E7599&7600

Figure 64.15
Calculated Stark profile of the He- β line of Kr^{34} (solid line) and the combined Stark and Doppler profile corresponding to an ion temperature of 10 keV (dashed line). Electron densities n_e of (a) $1 \times 10^{24} \text{ cm}^{-3}$ and (b) $5 \times 10^{24} \text{ cm}^{-3}$ were assumed.

transition is located at 15,451 eV, and the triplet-singlet transition is located at 15,426 eV. Additional peaks appear because of field mixing among the levels of the upper manifold.

Comparison of Figs. 64.15(a) and 64.15(b) clearly shows the effect of increasing density on the profile. The lower density, $1 \times 10^{24} \text{ cm}^{-3}$ ($\sim 4.5 \text{ g/cm}^3$), is at the upper end of the expected density range for the high-temperature target shots. The higher density, $5 \times 10^{24} \text{ cm}^{-3}$ ($\sim 22.5 \text{ g/cm}^3$), corresponds to future experiments where both high density and high temperature will be achieved. For the lower-density case the combined profile width is dominated by the Doppler broadening and can thus yield the ion temperature. To measure this width, a spectral resolution $\lambda/\Delta\lambda$ greater than ~ 1000 is required. This is not easily achievable with a flat crystal spectrometer, unless employed at a very large distance from

the target; however, a Rowland-circle focusing spectrograph can readily achieve this.⁵ In going from the lower density ($1 \times 10^{24} \text{ cm}^{-3}$) to the higher density ($5 \times 10^{24} \text{ cm}^{-3}$) the line width more than doubles, reflecting the increasing effect of the Stark broadening. It should be noted, however, that this broadening is mostly the result of the increase in intensity of forbidden components. Only at much higher densities will the total width of the manifold be determined by the Stark width rather than by the separation of the components. For the density range covered by Fig. 64.15, density signatures are provided by the width as well as the shape of the compound profile, which in turn is determined by the change in intensity and spectral position of the various components. In particular, in going from the lower to the higher density, the peak intensity of the compound profile shifts to lower energies by about 10 eV (due to the so-called "level repulsion" in second-order perturbation theory). To measure this shift, a spectral resolution $\lambda/\Delta\lambda$ greater than ~ 2000 is required.

Diagnosis of ρR using High-Opacity Lines

Optically thick spectral lines can be used to deduce the ρR of the compressed core. The self-absorption of spectral lines (i.e., the absorption by the same transition as that of the emission line) affects both the emergent line intensity as well as its spectral shape. Self-absorption leads to broadening; for a spatially uniform temperature the spectral profile will tend to be flat-topped, whereas for a radially falling temperature the line profile may have a central minimum. In the past, the broadening due to self-absorption of the Lyman- α line of argon was employed to estimate the core ρR .⁶ As explained in Ref. 6, the density has to be known (by fitting Stark profiles to an optically thin line) to deduce the ρR from an optically thick line. Alternatively, the width of several optically thick lines in the same line series must be measured.⁷ These methods can be employed here as well. However, we pursue an alternative method, based on the intensity of the optically thick line rather than its profile, which does not require a prior knowledge of the density or the use of additional lines.

The intensity of an optically thick line emerging from the plasma volume is related to the escape factor parameter, which has been the subject of numerous publications.⁸⁻¹¹ The escape factor G is defined by

$$G(\tau_0) = \int_{-\infty}^{\infty} P(\delta E) \exp[-\tau_0 P(\delta E)/P(\delta E = 0)] d(\delta E), \quad (1)$$

where δE is the energy separation from the unperturbed posi-

tion, $P(\delta E)$ is the line profile at δE in inverse energy units, and $\tau_0 = \tau(0)$ is the optical depth at $\delta E = 0$. The line opacity $\tau(\delta E)$ can be expressed as [see Eq. (8-14) in Ref. 12]

$$\tau(\delta E) = \left(\pi e^2 h / M m c \right) P(\delta E) f \rho R \varepsilon Q_n, \quad (2)$$

where M is the krypton ionic mass, m is the electron mass, e is the electron charge, h is Planck's constant, c is the speed of light, f is the absorption oscillator strength of the line, ρR is the total areal density (mostly that of the fuel), ε is the fraction of krypton in the fuel (by mass), and Q_n is the fraction of krypton ions in the absorbing level (i.e., the lower level of the transition). The spectral position $\delta E = 0$, which is somewhat arbitrary, is taken to be 15,451 eV, the unperturbed position of the strongest line.

The escape factor $G(\tau_0)$ in spherical geometry, as given by Eq. (1), corresponds to a point source at the center of the sphere, with τ_0 the opacity integrated over the radius. For a source uniformly distributed over the sphere, Mancini *et al.*¹¹ have shown that $G(\tau_0)$ for Holtsmarkian profiles and large opacities is about twice as large as for the point-source case. This indicates that knowing the temperature profile (or the spatial distribution of emitting and absorbing ions) is not critical when using the calculated escape factor for diagnostics. Thus, a two-temperature spatial profile (a hot spot

surrounded by a cool absorbing layer) and a uniform temperature profile give an escape factor that differs by only a factor of 2 for any $\tau_0 \gg 1$. To determine which geometry agrees better with the experiment we can examine two experimental signatures: (a) for a uniform source, the core image size at high photon energy will be about the same as that at low photon energy, whereas for a hot-spot source the former will be much smaller than the latter, and (b) for a uniform source the observed line profile will be flat-topped, whereas for a hot-spot source a self-reversal (or minimum) will be observed at the position of the profile peaks. Equation (1) applies to a two-temperature spatial profile but assumes that the line profile is the same in both the emission and absorption regions. This implies a uniform density since the density-dependent Stark broadening dominates the emergent profile for high opacities (see below). As an example, if the absorption line profile is half as wide as the emission profile (indicating a lower density by about a factor of 2.8), the escape factor can be shown to be larger by about 30%.

To obtain the escape factor $G(\tau_0)$ from Eq. (1) for our case, we use profiles such as those in Fig. 64.15. Figure 64.16 shows the escape factor as a function of the opacity at line center (15,451 eV), with and without the Doppler profile contribution. The curves are calculated for an ion temperature of 10 keV. The escape factor G depends on the temperature only through the Doppler contribution. Figure 64.16 shows that we

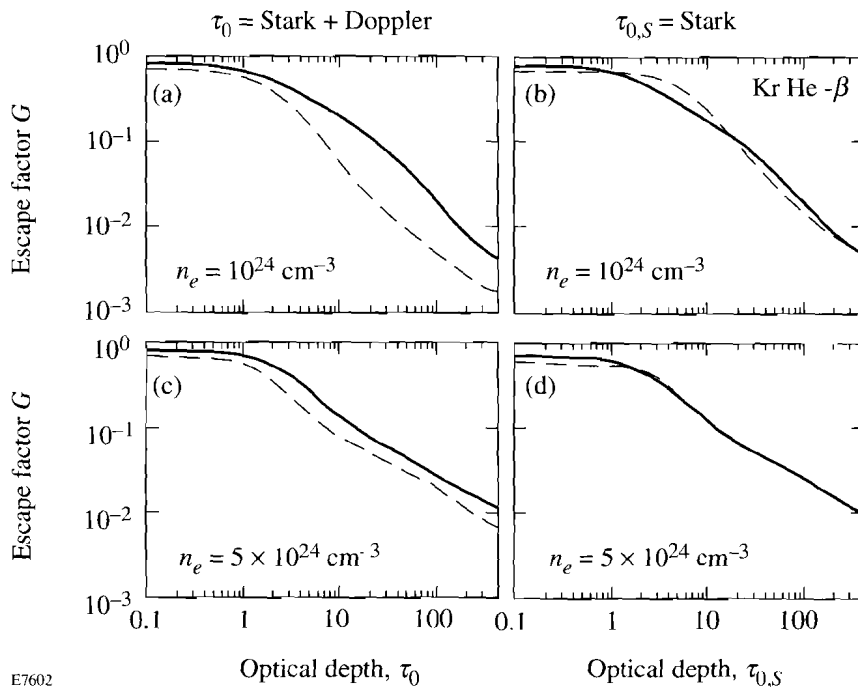


Figure 64.16
Calculated escape factor of the He- β line of Kr^{+34} for the two electron densities used in Fig. 64.15, as a function of the opacity at the line center (15,451 eV), without the Doppler contribution (solid curves) and with the Doppler contribution (dashed curves). In (a) and (c) the opacity τ_0 at 15,451 eV relates to the total Stark + Doppler profile, while in (b) and (d) the opacity $\tau_{0,S}$ at 15,451 eV relates to the Stark profile only.

E7602

can almost eliminate this dependence by plotting G as a function of $\tau_{0,S}$, the opacity at line center due to the Stark profile only. When changing from τ_0 to $\tau_{0,S}$, the curves of total profile shift to opacity values that are larger (since $\tau_{0,S} > \tau_0$) by the ratio $\tau_{0,S}/\tau_0$. The two curves thus plotted are almost coincident. The reason for this is simple: The Doppler profile decays much faster, with increasing separation from line center, than the Stark profile. Thus, the far wings are relatively unaffected by Doppler broadening. However, the escape factor for high opacity values depends only on the far wings [see Eq. (1)]. Therefore, the escape factor for high opacities will be relatively independent of the temperature. Since the profile on the far wings is essentially identical to the Stark profile, the escape factor will depend only on the Stark opacity $\tau_{0,S}$ at line center.

A similar situation will arise if we include ion-dynamic effects in the calculation of the Stark profiles. Effects on the Stark profile of the motion of perturbing ions (which are otherwise assumed stationary) will depend also on the ion temperature and will affect mostly the line center rather than its wings. Thus, the opacity $\tau_{0,S}$ relates to the Stark profile without either the Doppler effect or the ion-dynamic effects.

Comparison of the profiles in Fig. 64.16 shows also the relative insensitivity of the escape factor to the density. As mentioned earlier, for a Holtsmarkian profile and high opacities $G(\tau_0)$ depends only on τ_0 and not on the density (or the line width). For easier comparison, Fig. 64.17 shows the escape-factor curves from Figs. 64.16(b) and 64.16(d), calculated without the Doppler contribution, for the two densities $1 \times 10^{24} \text{ cm}^{-3}$ and $5 \times 10^{24} \text{ cm}^{-3}$. As seen, the two profiles overlap to within a factor of ~ 1.4 . Similar agreement is obtained in comparing curves that do include the Doppler broadening. We can thus use Fig. 64.16 to find the quantity $\tau_{0,S}$ from a measured value of the escape factor, without a precise knowledge of the temperature or the density. The question before us now is what does the opacity $\tau_{0,S}$ depend on, i.e., what diagnostic information can be inferred from knowing $\tau_{0,S}$?

From Fig. 64.16, the escape factor for high opacity in the density range $(1-5) \times 10^{24} \text{ cm}^{-3}$ can be approximated by the relation

$$G(\tau_{0,S}) \sim 1.3/(\tau_{0,S})^{0.9}. \quad (3)$$

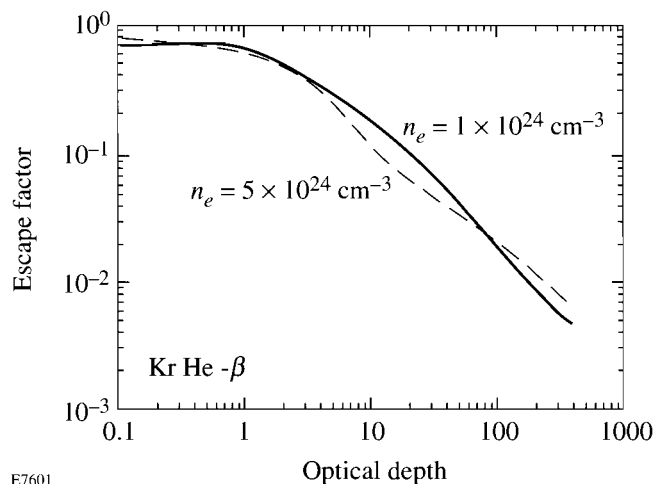


Figure 64.17
Calculated escape factor of the He- β line of Kr^{34} for two electron densities, as a function of the opacity at line center (15,451 eV), without the Doppler contribution.

Only at much higher densities, where level mixing of the $n = 3$ manifold due to the plasma electric field becomes substantial, will this relation tend to that for the Holtsmarkian profile mentioned above. For that case it was shown earlier¹ that the density dependence of $\tau_{0,S}$ drops out but the determination of $\tau_{0,S}$ (through the measurement of the escape factor) can then yield information on possible mixing. For the density range discussed here, Eq. (3) does lead to a dependence of $\tau_{0,S}$ on the density (or on the ρR), thus providing a diagnostic for ρR . A method for measuring the escape factor was described in Ref. 1.

The diagnostic method for the fuel ρR consists of measuring the escape factor as outlined in Ref. 1, and then deducing $\tau_{0,S}$ from curves like those in Fig. 64.16. It follows from the definition of τ_0 (Eq. 2) that if we substitute $\tau_{0,S}$ for τ_0 , the profile $P(\delta E = 0)$ appearing in Eq. (2) should refer to the pure Stark profile $P_S(\delta E = 0)$. This profile can be read off the calculated Stark profiles such as those in Fig. 64.15 and is obviously a function of the density. In the range $(1-5) \times 10^{24} \text{ cm}^{-3}$, $P_S(\delta E = 0)$ as a function of the density ρ can be approximated as

$$P_S(\delta E = 0) \sim 0.4/\rho^{0.88}. \quad (4)$$

In any practical case, the complete profile curves can be used rather than this approximate expression. Further, in an imploding spherical target the following relationship holds:

$$\rho R = (3M_F/4\pi)^{1/3} \rho^{2/3}, \quad (5)$$

in terms of the total fill mass M_F (fuel and krypton). Combining Eqs. (2), (4), and (5) we can write

$$\rho R = 0.02A^{3.125} (3M_F/4\pi)^{1.375} G^{3.437}, \quad (6)$$

where $A = (\pi e^2 h / M m c) f \epsilon Q_n$ [from Eq. (2)]. The quantity Q_n has been shown¹ to be very close to unity over a wide temperature range. This relation is the basis for determining the fuel ρR from a measurement of the escape factor G . As mentioned above, actual calculated curves can be used rather than the approximations given in Eqs. (3) and (4).

Finally, we estimate the expected sensitivity of the method for measuring the fuel ρR . To find G from the intensity ratio of the helium- β and Balmer- α lines,¹ with a precision of $\pm 20\%$, the intensity of each of the lines (in relative units) has to be measured with a precision of $\pm 10\%$. A method for the relative calibration of the two instruments measuring the two different wavelengths was described in Ref. 1. From Eq. (3), an error of $\pm 20\%$ in G will result in an error of $\pm 22\%$ in $\tau_{0,S}$. Finally, from Eq. (6), the precision in determining the compressed fuel ρR will be better than a factor of 2.

Summary

In summary, the use of krypton doping for diagnosing high-temperature, medium-density implosions has been discussed for two cases: low-opacity lines (achieved with low doping) and high-opacity lines. Using detailed Kr Stark profile calculations, it is found that the profiles of low-opacity lines in the expected density range are dominated by Doppler broadening; they can thus provide a measurement of the ion temperature if spectrometers of spectral resolution $\Delta\lambda/\lambda \geq 1000$ are used. For high-opacity lines, obtained with a higher krypton fill pressure, the measurement of the escape factor can yield the ρR of the compressed fuel. At higher densities, Stark broadening of low-opacity lines becomes important and can provide a measurement of the density, whereas lines of higher opacity can be

used to estimate possible mixing.¹ These higher densities will arise in future experiments where high temperatures and high densities will be simultaneously achieved.

ACKNOWLEDGMENT

This work was supported by the U.S. Department of Energy Office of Inertial Confinement Fusion under Cooperative Agreement No. DE-FC03-92SF19460, the University of Rochester, and the New York State Energy Research and Development Authority. The support of DOE does not constitute an endorsement by DOE of the views expressed in this article.

REFERENCES

1. Laboratory for Laser Energetics LLE Review **61**, NTIS document No. DOE/SF/19460-58, 1994 (unpublished), p. 1.
2. L. A. Woltz and C. F. Hooper, Jr., *Phys. Rev. A* **38**, 4766 (1988).
3. R. C. Mancini *et al.*, *Comput. Phys. Commun.* **63**, 314 (1991).
4. R. D. Cowan, *The Theory of Atomic Structure and Spectra* (University of California Press, Berkeley, CA, 1981).
5. J. C. Kieffer *et al.*, *Appl. Opt.* **28**, 4333 (1989); B. Yaakobi, T. Boehly, and P. Audebert, *Rev. Sci. Instrum.* **61**, 1915 (1990).
6. B. Yaakobi, S. Skupsky, R. L. McCrory, C. F. Hooper, H. Deckman, P. Bourke, and J. M. Soures, *Phys. Rev. Lett.* **44**, 1072 (1980).
7. N. D. Delameter *et al.*, *Phys. Rev. A* **31**, 2460 (1985).
8. F. E. Irons, *J. Quant. Spectrosc. Radiat. Transfer* **22**, 1 (1979).
9. J. P. Apruzese, *ibid.* **34**, 447 (1985).
10. C. Chenais-Popovics *et al.*, *ibid.* **36**, 355 (1986).
11. R. C. Mancini, R. F. Joyce, and C. F. Hooper, Jr., *J. Phys. B: At. Mol. Phys.* **20**, 2975 (1987).
12. H. R. Griem, *Plasma Spectroscopy* (McGraw-Hill, New York, 1964).